ISBN: 978-3-95450-201-1 doi:10.18429/JACoW-IBIC2018-WEOC03

A SIMPLE MODEL TO DESCRIBE SMOKE RING SHAPED BEAM PROFILE MEASUREMENTS WITH SCINTILLATING SCREENS AT THE EUROPEAN XFEL

G. Kube, S. Liu, A. Novokshonov, M. Scholz, DESY, Hamburg, Germany

Abstract

Standard beam profile measurements of high-brightness electron beams based on optical transition radiation (OTR) may be hampered by coherence effects induced by the micro–bunching instability which render a direct beam imaging impossible. For the European XFEL it was therefore decided to measure transverse beam profiles based on scintillating screen monitors using LYSO:Ce as scintillator material. While it is possible to resolve beam sizes down to a few micrometers with this kind of scintillator, the experience during the commissioning of the XFEL showed that the measured emittance values were significantly larger than the expected ones. In addition, beam profiles measured at bunch charges of a few hundreds of pico-Coulomb show a 'smoke ring' shaped structure. While coherent OTR emission and beam dynamical influence can be excluded to explain this observation, it is assumed that the beam profile distortions are caused by effects from the scintillator material. A simple model is presented which takes into account quenching effects of excitonic carriers inside a scintillator in a heuristic way. Based on this model, the observed beam profiles can be understood qualitatively. Together with the model description, first comparisons with experimental results are presented.

INTRODUCTION

Transverse beam profile diagnostics in electron linacs is widely based on optical transition radiation (OTR) as standard technique which is observed in backward direction when a charged particle beam crosses the boundary between two media with different dielectric properties. Unfortunately, microbunching instabilities in high–brightness electron beams of modern linac–driven free–electron lasers (FELs) can lead to coherence effects in the emission of OTR, thus rendering it impossible to obtain a direct image of the particle beam and compromising the use of OTR monitors as reliable diagnostics for transverse beam profiles. The observation of coherent OTR (COTR) has been reported by several facilities (see e.g. Ref. [1]), and in the meantime the effect of the microbunching instability is well understood [2].

For the European XFEL it was therefore decided to use scintillation screen monitors because the light emission in a scintillator is a multistage stochastic process from many atoms which is completely insensitive to the longitudinal bunch structure. In a series of test measurements performed in the past few years, the applicability of inorganic scintillators for high resolution electron beam profile measurements was investigated [3, 4]. Most notably, the dependency of the resolution on the scintillator material and on the observation geometry was studied with respect to resolve beam profiles in the order of several tens of micrometers, and it was concluded that LYSO ($Lu_{2(1-x)}Y_{2x}SiO_5$:Ce) is a suitable material because it gives the best spatial resolution. Based on these measurements, screen monitor stations were designed for the European XFEL using 200 µm thick LYSO screens [5]. In a high resolution beam profile measurement using an XFEL–type screen it was demonstrated that it is possible to resolve a vertical beam size of $\sigma_y = 1.44\,\mu m$ [6].

However, the experience during the commissioning of the XFEL showed that the measured emittance values were significantly larger than the expected ones [7, 8]. In addition, beam profiles measured at bunch charges of a few hundreds of pico-Coulomb show a 'smoke ring' shaped structure, see e.g. Fig. 1. While the contribution of COTR emission

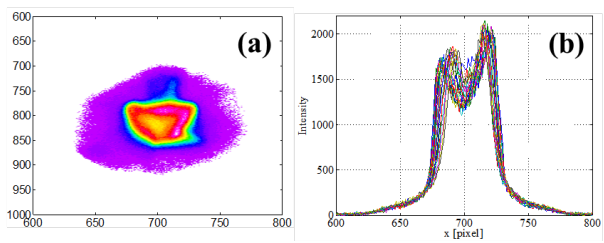

Figure 1: (a) Typical smoke ring shaped beam profile as measured with an XFEL screen monitor based on a 200 µm thick LYSO screen. (b) Various horizontal cuts through the 2D–profile demonstrate the intensity drop in the central part of the beam spot.

from the scintillator surface, beam dynamical influence, and camera effects could be excluded to explain this observation, it is assumed that the beam profile distortions are caused by effects from the scintillator material.

In the following a simple model is described which takes into account quenching effects of excitonic carriers inside a scintillator in a heuristic way. Based on this model, the observed beam profiles can be understood qualitatively.

BASIC CONSIDERATIONS

Degradation effects in scintillator based beam profile measurements are reported in a number of publications, see e.g. Refs. [9–13]. The scintillator influence is mainly interpreted as saturation of the measured profiles, caused e.g. by full excitation of the luminescent centers in some regions inside the scintillator. While inspecting Fig. 1 it is obvious that the XFEL observations cannot simply be described by a saturation effect which would result in a flattening of the measured beam profiles. It rather leads to the conclusion

ISBN: 978-3-95450-201-1 doi:10.18429/JACoW-IBIC2018-WEOC03

that luminescent centers may even be quenched in the central part of the beam spot such that the scintillating light intensity is decreased in these regions.

Taking into account the experience of high energy physics, it is known that scintillator based electron calorimeters posses a non–linear energy resolution, and the degree of non–linearity depends on the scintillator material. Following the explanations e.g. in Ref. [14] this effect can be attributed to the ionization density inside the material: In the primary interaction of a particle with the calorimeter material an electromagnetic shower is generated, and the shower particles create excitonic states (electron/hole or e/h pairs, excitons ...) inside the scintillator material. As the shower particles slow down, the ionization density increases as described by the kinematical factor $\propto \beta^{-2}$ (with $\beta = v/c$) of the Bethe–Bloch equation such that the initial part of the particle track has lower ionization density than the final portion of the track. The light output in a scintillator depends on the ionization density, if the density is above a critical limit excitonic states can annihilate in an Auger–like process without creating a scintillating photon. As a result, the relative light yield in a scintillator typically decreases with decreasing electron energy, see e.g. Ref. [15] and the figures therein. As shown in Fig. 1 of this reference, the light yield of a LSO:Ce scintillator (which has very similar properties than a LYSO:Ce scintillator, the small yttrium contribution of $x \sim 0.1$ simply serves to stabilize the crystal growth by the Czochralski method and to reduce the production costs [16]) exhibits a strong non-linear behavior which seems to be a general property of the class of "Silicates" as LSO, YSO, LPS where the oxygen is intimately bound to the silicon as a SiO_4^{4-} moiety [15].

To be more precise, the general scheme of relaxation of electronic excitations in crystalline scintillators can be subdivided in 5 stages [17], (1) the energy conversion and e/h generation via inelastic scattering, (2) the thermalization of the e/h pairs, (3) their localization, i.e. e/h capturing at traps, (4) the energy transfer to the luminescent centers, and (5) their radiative relaxation. Following Refs. [14, 17] it is stage (4) which causes the non–linearity in the scintillator light yield. Therefore, improving the linearity of a scintillator should in principle correlate with the minimization of the interaction time of excitonic states.

SCINTILLATOR MODEL

In the following the principal considerations from the previous section are transferred to the field of beam profile diagnostics of ultra–relativistic electron beams. Main idea is that the ionization track density which is responsible for the non–linear scintillator behavior is determined by the primary beam particle density rather than by the secondary energy of shower particles. Because of the similarity between LSO and LYSO scintillators, in the subsequent estimations LSO is used due to the simpler chemical composition.

If an ultra–relativistic electron beam traverses a scintillator it generates ionization and radiative losses. However, the Bremsstrahlung mean free path length in a LSO scintillator can be estimated to 1.24 mm which is much larger than the scintillator thickness of 200 µm as it is the case for the LYSO screens at the XFEL. Therefore, electromagnetic shower generation is strongly suppressed and energy conversion and e/h generation in stage (1) are simply governed by the collisional stopping power. For ultra–relativistic electron energies, the stopping power is in the region of the Fermi–plateau and the energy loss of about $\Delta E = 266$ keV in a 200 µm LSO scintillator is negligible compared to GeV beam energies.

In a classical picture the onset of the Fermi–plateau is described as cancellation of the incoming particle field by the induced polarization field of the electrons in the medium, thus giving a measure for the transverse extension of the e/h formation region. According to Ref. [18] the particle field extension has a limiting value of $R_\delta = c/\omega(1-\varepsilon)^{-1/2} \approx c/\omega_p$ using the simplified model of a free–electron gas with ω_p the plasma frequency which amounts to $R_\delta = 3.85$ nm in the case of a LSO scintillator. In the following R_δ is used as estimate for the radius determining the ionization density. Furthermore, taking into account multiple scattering inside a 200 µm thick LSO scintillator, with about 900 scattering events the mean path length between individual scattering is much larger than R_δ. Moreover, considering characteristic interaction time scales, the particle flight time through the scintillator and the bunch length of an uncompressed bunch are $\leq 10^{-12}$ sec while dynamical processes in scintillator take place in the order of 10^{-12}–10^{-10} sec. With respect to the particle beam dynamics, in the subsequent model the passage of a single electron through the scintillator is therefore described by the generation of a static ionization tube with radius R_δ which is homogeneously filled with e/h pairs.

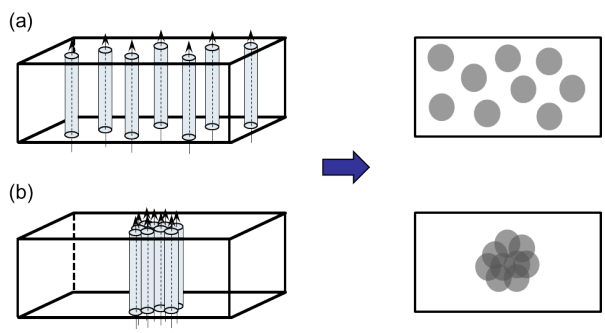

Figure 2: Passage of individual electrons through a scintillator in the case of (a) low and (b) high particle density. Each electron creates a homogeneous ionization tube. Due to the static behavior of the ionization tubes a two–dimensional representation is sufficient.

The situation is schematically depicted in Fig. 2 for the case of a beam with low and with high particle density. Due to the static behavior of the ionization tubes, for the description of the ionization track density a two–dimensional representation is sufficient as shown on the right side of this

ISBN: 978-3-95450-201-1 doi:10.18429/JACoW-IBIC2018-WEOC03

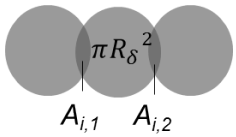

Figure 3: The ionization track density n_t is geometrically estimated by the ionization tube area and the sum of the track intersections: $n_t \propto \pi R_\delta^2 + \sum_k A_{i,k}$

figure. In order to estimate the particle track density in the case of a beam with high particle density, a simple geometrical model is used which is based on the 2D–representation. As shown in Fig. 3 the cross section of each ionization tube is described by a circle with area πR_δ^2. If the particle density is high, individual ionization tubes may overlap and the track density is simply estimated as the sum of tube area and track intersections.

The calculation of a distorted beam profile then consists of four consecutive steps. In the first step the transverse particle beam profile (which is assumed to be Gaussian in the following) is transformed into a 2D surface density profile describing the local particle density $\sigma(x, y)$. Assuming an adiabatic change in the local density concentration, in the second step the mean distance between the ionization tubes $D(x, y)$ is calculated considering the nearest neighbor distribution according to $D(x, y) = \frac{1}{2}\sigma^{-1/2}(x, y)$, see the formalism described in Ref. [19]. In the next step, with knowledge of the mean distance between the ionization tubes a regular grid of neighboring tubes is constructed and the local ionization track density $n_t(x, y)$ is geometrically estimated as described above. Finally, for each point of the beam profile a weighting factor $w(x, y)$ is calculated

$$w(x, y) = \frac{1}{1 + \alpha \frac{dE}{dx}(x, y)}$$

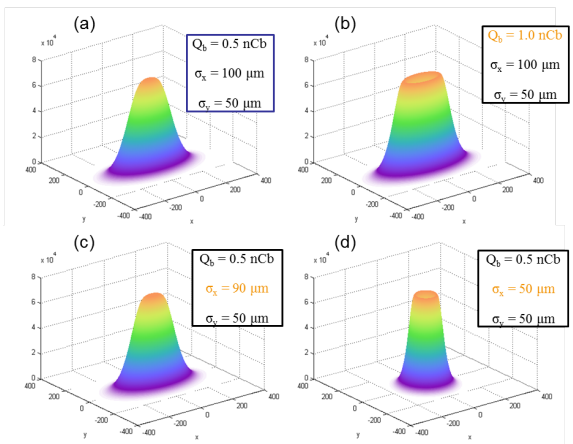

Figure 4: Calculated beam profiles according to the model described in this work. Starting with typical XFEL beam parameters (a) and assuming that $\alpha = 6.4 \times 10^{-5}$, beam profiles for increased bunch charge (b) or decreased horizontal beam size (c,d) are shown.

which is similar to the formula of Birks [20] describing the non–linearity in the scintillator light yield. Here it is assumed that $\frac{dE}{dx} \propto n_t^3$ and α is a freely adjustable parameter describing the quenching strength.

MODEL CALCULATION

Figure 4 shows calculated beam profiles according to the model presented in this work. Starting with a Gaussian beam profile and typical XFEL beam parameters (a) it can be seen that both increasing the bunch charge (b) and reducing the beam size (c,d) may result in a pronounced beam profile degradation which is caused by an increase in the local ionization track density in the central part of the beam interaction region with the scintillator. Thereby it is possible to produce smoke ring shaped beam profiles as observed at the XFEL.

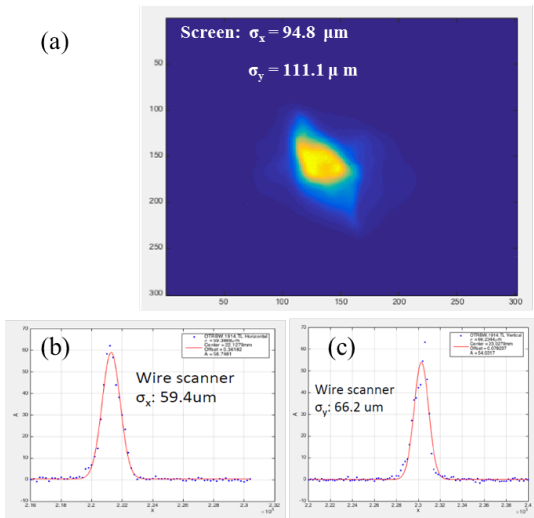

Figure 5: Beam profile measurements with the XFEL screen monitor (a) and wire scanner system (b,c), taken at the same location for the same beam parameters.

In the next step a profile measurement taken at the XFEL is directly compared to the presented scintillator model. Fig. 5(a) shows a profile measurement taken with a screen monitor together with the fit results for the projected horizontal and vertical intensity distributions, assuming Gaussian profiles. In addition, wire scanner profile scans are plotted below (b,c) which were taken at the same location and for the same beam parameters with the XFEL wire scanner system described in Ref. [21]. As can be seen, the screen monitor based analysis systematically overestimates the transverse beam sizes. However, using the wire scanner beam sizes as input for the scintillator model calculation, a 2D beam profile was calculated. A fit of the calculated horizontal and vertical intensity projections results in beam sizes of $\sigma_x = 97\,\mu\text{m}$ and $\sigma_y = 108\,\mu\text{m}$ which is close to the measured sizes from the screen monitor, c.f. Fig. 5(a). Thus the proposed scintillator model is able to produce smoke ring shaped beam profiles with beam sizes close to the measured ones. However, the calculated beam shape strongly depends

ISBN: 978-3-95450-201-1 doi:10.18429/JACoW-IBIC2018-WEOC03

on the quenching parameter α which is freely selectable up to now.

SUMMARY AND OUTLOOK

Based on to the observation of smoke ring shaped beam profiles using the screen monitor stations at the XFEL which utilize LYSO as scintillator material, a simple model is presented which takes into account quenching effects of excitonic carriers inside a scintillator in a heuristic way. Following the experience of calorimetry in high energy physics, the main idea is that the ionization track density which is responsible for non–linear scintillator behavior is determined by the primary beam particle density. The track density is estimated using simple geometrical considerations for the ionization tubes which are generated from beam particles crossing the scintillator. With the help of the proposed scintillator model it is possible to reproduce smoke ring shaped beam profiles as observed at the XFEL, the level of quenching in the central part of the beam generated spot in the scintillator depends on bunch charge and beam size, i.e. it is controlled by the particle density. Moreover, the discrepancy in extracted beam sizes between a screen and a wire scanner measurement can be explained based on this model. However, so far the quenching parameter α is freely adjustable in the model. Presently studies are under way in order to get a better insight into the underlying physical processes.

In order to support the assumption that the quenching of excitation centers causes smoke ring shaped beam profiles, it is again referred to the experience of the scintillator community for high energy physics. In Ref. [15] scintillator electron response measurements from 29 screen materials are compiled and fitted based on a model combining different theories. One of the fit parameters, $(\mathrm{d}E/\mathrm{d}x)_{\mathrm{BIRKS}}$, characterizes the effect of exciton–exciton quenching, materials with a low magnitude of this parameter experience greater annihilation. Comparing this parameter for LSO and for YAG which is widely used in particle beam diagnostics, with $(\mathrm{d}E/\mathrm{d}x)_{\mathrm{BIRKS}}$ = 133–185 MeV/cm for LSO:Ce (depending on the doping level) compared to 526 MeV/cm for YAG:Ce the first material should exhibit much stronger non–linearity and should be prone to smoke–ring shaped beam spots. Figure 6 shows a comparison of beam spot measurements taken under the same experimental conditions at the XFEL. As can be seen, the LYSO screen measurement shows indeed a clear signature of a smoke ring while the YAG measurement is unaffected.

Finally the question for suitable scintillator materials for beam profile diagnostic applications remains open. In the case of hadron beams the question is especially difficult to tackle. Due to the higher rest masses the beam particles usually have a much higher energy loss according to the Bethe–Bloch equation such that even individual particle tracks may be prone to excitation quenching. In the case of ultra relativistic electron beams one can refer again to the compilation in Ref. [15] where LuAG doped either with Ce or Pr exhibits a very high $(\mathrm{d}E/\mathrm{d}x)_{\mathrm{BIRKS}}$ such that the

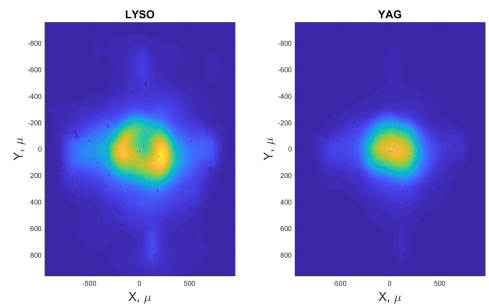

Figure 6: Beam spots measured with a screen monitor station using a LYSO (left) and a YAG scintillator (right) for the same beam parameters. Both screens are mounted in the same station.

exciton–exciton quenching should be small. However , the resolution study performed in Ref. [4] showed that the spatial resolution of a LuAG scintillator was worse compared to a LYSO screen. Therefore other materials could be more promising. As already mentioned before, improving the linearity of a scintillator should in principle correlate with the minimization of the interaction time of excitonic states. In this context scintillator materials where gadolinium is stochiometrically incorporated in the crystal structure seem to be promising [15]. In these materials it is assumed that excitation carriers can rapidly transfer their energy to excited states of gadolinium, and a rapid migration of this energy among the Gd sub–lattice is expected until a Ce doping ion is reached. According to Ref. [22] YAP could also be an interesting material because it exhibits a high mobility of excitonic carriers which may reduce the quenching probability. A first study with YAP was already performed at the XFEL, the screen material shows indeed better linearity and resolution compared to LYSO, cf. Fig. 7. However, the light yield of YAP is rather low. Presently more detailed studies are in preparation and different scintillator materials like YAG, YAP, LuAG, and GGAG will be investigated in view of linearity and resolution.

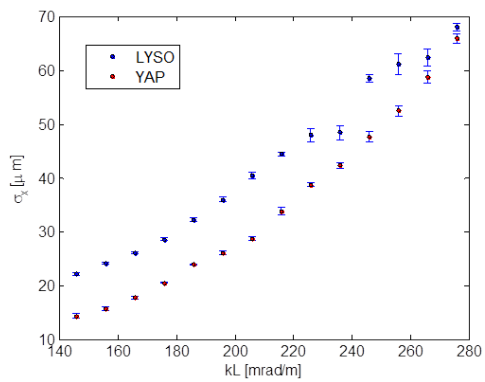

Figure 7: Comparative resolution study using a YAP:Ce and a LYSO:Ce scintillator at the XFEL. The measurements were taken under the same experimental conditions.

ISBN: 978-3-95450-201-1 doi:10.18429/JACoW-IBIC2018-WEOC03

REFERENCES

[1] S. Wesch and B. Schmidt, Proc. DIPAC'11, Hamburg, Germany, May 2011, WEOA01, p.539 (2011).

[2] G. Stupakov, Proc. IPAC'14, Dresden, Germany, June 2014, THYA01, p.2789 (2014).

[3] G. Kube, C. Behrens, W. Lauth, Proc. IPAC'10, Kyoto, Japan, May 2010, MOPD088, p.906 (2010).

[4] G. Kube *et al.*, Proc. IPAC'12, New Orleans (Louisiana), USA, May 2012, WEOAA02, p.2119 (2012).

[5] Ch. Wiebers, M. Holz, G. Kube *et al.* Proc. IBIC'13, Oxford, UK, September 2013, WEPF03, p.807 (2013).

[6] G. Kube *et al.*, Proc. IBIC'15, Melbourne, Australia, September 2012, TUPB012, p.330 (2015).

[7] B. Beutner, Proc. FEL'17, Santa Fe (New Mexico), USA, August 2017, WEA01, p.381 (2017).

[8] D. Nölle, *The Diagnostic System at the European XFEL; Commissioning and First User Operation*, these proceedings, TUOA01.

[9] A. Murokh *et al.*, in *The Physics of High Brightness Beams*, World Scientific (2000), p. 564.
A. Murokh *et al.*, Proc. PAC'01, Chicago, USA, June 2001, TPAH049, p. 1333 (2001).

[10] T.F. Silva *et al.*, Proc. PAC'09, Vancouver, Canada, May 2009, TH6REP040, p. 4039 (2009).

[11] U. Iriso *et al.*, Proc. DIPAC'09, Basel, Switzerland, May 2009, TUPB15, p. 200 (2009).

[12] F. Miyahara et al., Proc. IPAC'17, Copenhagen, Denmark, May 2017, MOPAB067, p. 268 (2017).

[13] R. Ischebeck *et al.*, FEL'17, Santa Fe (New Mexico), USA, August 2017, WEP039 (unpublished).

[14] W.W. Moses *et al.*, IEEE Trans. Nucl. Sci. **55** (2008) 1049.

[15] S.A. Payne *et al.*, IEEE Trans. Nucl. Sci. **58** (2011) 3392.

[16] D.W. Cooke *et al.*, J. Appl. Phys. **88** (2000) 7360.

[17] A.N. Vasil'ev, Proc. SCINT'99, Moscow, Russia, August 1999, p.43 (1999).

[18] W.W.M Allison, J.H. Cobb, Ann Rev. Nucl. Part. Sci. **30** (1980) 253.

[19] S. Chandrasekhar, Rev. Mod. Phys. **15** (1943) 1.

[20] J.B. Birks, Proc. Phys. Soc. **A64** (1951) 874.

[21] T. Lensch, *The European XFEL Wire Scanner System*, these proceedings, WEPC05.

[22] Q. Li *et al.*, J. Appl. Phys. **109** (2011) 123716.